Article

Dentate gyrus norepinephrine ramping facilitates aversive contextual processing

Eric T. Zhang[1,2], Grace S. Saglimbeni[2], Jiesi Feng[3], Yulong Li[3] & Michael R. Bruchas[1,2,4,5] ✉

Dysregulation in aversive contextual processing is believed to affect several forms of psychopathology, including post-traumatic stress disorder (PTSD). The dentate gyrus (DG) is an important brain region in contextual discrimination and disambiguation of new experiences from prior memories. The DG also receives dense projections from the locus coeruleus (LC), the primary source of norepinephrine (NE) in the mammalian brain, which is active during stressful events. However, how noradrenergic dynamics impact DG-dependent function during contextual discrimination and pattern separation remains unclear. Here, we report that aversive contextual processing in mice is linked to linear elevations in tonic norepinephrine release dynamics within the DG and report that this engagement of prolonged norepinephrine release is sufficient to produce contextual disambiguation, even in the absence of a salient aversive stimulus. These findings suggest that spatiotemporal ramping characteristics of LC-NE release in the DG during stress likely serve an important role in driving contextual processing.

On any given day, humans must consistently engage in contextual learning processes such as pattern separation and contextual discrimination, as we experience new episodic events and compare novel information to previous experiences. These processes are critical for homeostatic cognitive and affective behavior, while deficits in this functioning are thought to underlie multiple neuropsychiatric disease states including post-traumatic stress disorder (PTSD) and schizophrenia[1–3]. These disorders are characterized by a dysregulation of pattern separation, and individuals with these disorders often experience elevated levels of fear and anxiety resulting from failures in contextual processing between incoming episodic information and existing memories, hypervigilance, and exaggerated threat detection[4–6]. Current therapeutic strategies to treat the resulting disorders are limited, although adrenergic receptor antagonists have been recently used with some positive effects[7,8]. Further research implicates the need for a deeper understanding of the neuromodulatory neural mechanisms behind contextual processing, to open translational opportunities for therapeutic development.

The hippocampus is a critical neural structure that mediates learning and memory and is involved in the processing of incoming environmental information[9–13]. Moreover, the dentate gyrus (DG), a subregion of the hippocampus, has been closely linked to contextual learning and pattern separation, wherein information from existing memories is compared to new incoming information[14–17]. In addition, the DG has been shown to be highly modulated by stress and aversive stimuli[18–20]. However, the mechanisms for this remain unresolved. Specifically, how do disrupted memory retrieval and failures in pattern separation give rise to contextual generalization in response to aversive stimuli?

One potential source of modulation for the DG is the locus coeruleus (LC), which provides dense innervations to the DG[21,22]. The LC, also known as the 'blue spot', is a small region located in the brain stem that supplies the mammalian brain with norepinephrine (NE) and has

[1]Department of Bioengineering, University of Washington, Seattle, WA, USA. [2]Department of Anesthesiology and Pain Medicine, University of Washington, Seattle, WA, USA. [3]State Key Laboratory of Membrane Biology, Peking University School of Life Sciences, Beijing, China. [4]Department of Pharmacology, University of Washington, Seattle, WA, USA. [5]Center for the Neurobiology of Addiction, Pain and Emotion, University of Washington, Seattle, WA, USA. ✉e-mail: mbruchas@uw.edu

been implicated in regulation of anxiety[23–26]. LC-NE tonic activity increases in response to stressful events and is necessary and sufficient for aversive behavior, leading to selective modulation of several brain structures, including the DG[27–31]. However, it is not known how LC-NE dynamics modulate the DG in memory-related disorders, nor what the temporal release properties of NE are in this behavior.

Here, we conducted an integrated neuromodulatory circuit analysis approach, combining optogenetic tools, in vivo fiber photometry, and a NE-selective biosensor with a well-established Pavlovian contextual fear discrimination (CFD) paradigm in which animals were placed in two similar, but different, contexts daily[12,17,32]. Elucidating the spatiotemporal dynamics of LC-NE modulation of DG-dependent aversive contextual processing provides critical information toward efforts to combat the dysregulation of contextual disambiguation in mental health disorders such as PTSD and schizophrenia.

Results

Linear elevations of tonic NE release within the DG occur during successful contextual discrimination of an aversive context

To elucidate the spatiotemporal dynamics of NE in the DG during behavior, we first injected novel biosensor $GRAB_{NE}$, a GPCR activation-based NE sensor with high specificity for NE, into the DG of Dbh-cre mice (Fig. 1a, b)[33]. We then implanted optical fibers above the injection sites for photometry recordings during behavioral tasks including tail lift, foot shock, and optogenetic stimulation (Fig. 1c). To determine the expression and efficacy of the $GRAB_{NE}$ biosensor in each animal to be examined, mice first underwent tail lift and foot shock testing for NE release calibration across animals. During the tail lift, we observed a significant increase in $GRAB_{NE}$ fluorescence during the tail lift compared to YFP controls (Fig. 1d, e). This signal began to rise significantly when the animal was first picked up by the tail, increased continuously while the animal was suspended for 20 seconds, and decreased back to baseline after the animal was returned to the ground. This outcome matches the dynamics recorded in the lateral hypothalamus during the initial development and characterization of $GRAB_{NE}$[33]. During foot shock, we also observed a significant increase in $GRAB_{NE}$ fluorescence compared to YFP controls (Fig. 1f, g). This signal increased sharply during the 2 s shock and decreased rapidly back to baseline following the termination of the shock. These results indicate successful calibration of $GRAB_{NE}$ for detecting spatiotemporal dynamics of endogenous NE release from LC to DG during stressful stimuli, allowing for potential use in our contextual fear discrimination task.

We then injected $GRAB_{NE}$ into the DG with optical fibers above the injection site of Dbh-cre mice, which then underwent an established contextual fear discrimination task (Fig. 1h)[12,17,32]. On day 1, mice displayed no significant differences in NE dynamics during the first 180 s of each context, while on days 5 and 9 there was sustained release of NE through the first 180 s in context A, while no such elevated release was observed in the safe context B (Fig. 1i, j). These mice also showed robust phasic increases in NE release in response to the 2 s foot shock on both day 1 and day 9 of training. In addition, while on day 1 there were no significant differences in freezing in context A compared to context B, on day 5 and day 9 there was a significantly increased amount of freezing in context A as compared to context B, indicating that mice successfully discriminated between the unsafe and safe contexts following training (Fig. 1k). To quantify the amount of NE released in both context A and context B, a total rate of change or "area under the curve (AUC)" was calculated, taking the AUC for each mouse in the first 180 s of both context A and context B. The amount of NE released in context A was significantly higher than in context B during the middle and late stages of training, while there was no significant difference in AUC between the two contexts in the early stages of training (Fig. 1l). These findings indicate that as mice were increasingly able to distinguish between the safe and unsafe contexts, there was a corresponding increase in NE release in the unsafe context compared

to the safe context. To quantify the correlation between these two factors, we calculated a ratio between the proportion of freezing behavior in context A (unsafe) compared to context B (safe), and the change in AUC (ΔAUC) in context A (unsafe) compared to context B (safe). We used linear regression and Pearson correlation to assess the link between these parameters for both the beginning and end of training (Supplementary Fig. 1a). While there is little to no significant relationship between the two variables at the beginning of training, by the end of the task this shifts to a significant fit between freezing ratio and ΔAUC in the two contexts. This indicates that mice that were better able to disambiguate between context A and context B also experienced higher amounts of prolonged NE release in the DG during the CFD task while in the unsafe context. In addition, we calculated the peak response during the last 17 s in each context, to quantify the response to foot shock in context A and saw a significantly higher peak response in context A compared to context B, indicating increased NE release in response to the aversive stimulus (Fig. 1m). However, when we used Pearson correlation to assess potential links between the difference in peak response in context A compared to context B with freezing ratio, there were no significant correlations between these two factors (Supplementary Fig. 1b). In addition, we calculated the slope of the NE dynamics, finding significant differences in slope between context A and context B during the middle and end stages of training, but not the beginning (Fig. 1n). We also tested mice injected with eYFP, in order to ensure that the increases seen during our CFD were in fact increases in NE release, rather than changes in fluorescence levels (Supplementary Fig. 1c, d). While these mice were able to successfully discriminate between context A and context B by the end of training, they did not display any differences in NE release between context A and context B by the end of training, both during the first 180 seconds of the trial and in response to the foot shock (Supplementary Fig. 1e–h). When examining potential links between the freezing ratio and AUC and between the freezing ratio and peak response via Pearson correlation, there were no significant correlations between these factors (Supplementary Fig. 1i, j). These results suggest that the differences observed during contextual fear discrimination were, in fact, due to prolonged NE release in the DG, detected by $GRAB_{NE}$.

We next sought to understand how NE dynamics persisted following successful discrimination in the CFD task and removal of the aversive stimuli, by observing NE signaling during a modified CFD extinction task (Supplementary Fig. 2a, b). In this task, following completion of the standard CFD task, mice underwent two additional days of training in which they were exposed to context B, then context A, for 15 min, with no shock in either context. In this task, mice successfully discriminated between context A and context B on both day 5 and day 9 of training, demonstrating successful learning, and continue to display significantly increased freezing in context A compared to context B on Day 10, while on Day 11 these mice no longer show significant differences in freezing between the two contexts. (Supplementary Fig. 2c). On day 1, mice displayed no significant differences in NE dynamics during the first 180 s of each context, while on days 5 and 9 there was sustained release of NE through the first 180 s in context A, while no such elevated release was observed in the safe context B (Supplementary Fig. 2d, e). These mice also showed robust phasic increases in NE release in response to the 2 s foot shock on both day 1 and day 9 of training. On day 10 of training, mice continued to display increased NE release in context A compared to context B, with NE levels remaining elevated through the entirety of the 15-minute trial, while on day 11, there were no significant differences in NE levels between the two contexts (Supplementary Fig. 2f, g). To quantify the total amount of NE released in both context A and context B over time, an area under the curve (AUC) analysis was used, taking the AUC for each mouse in the first 180 seconds of both context A and context B. The amount of NE released in context A was significantly higher than in
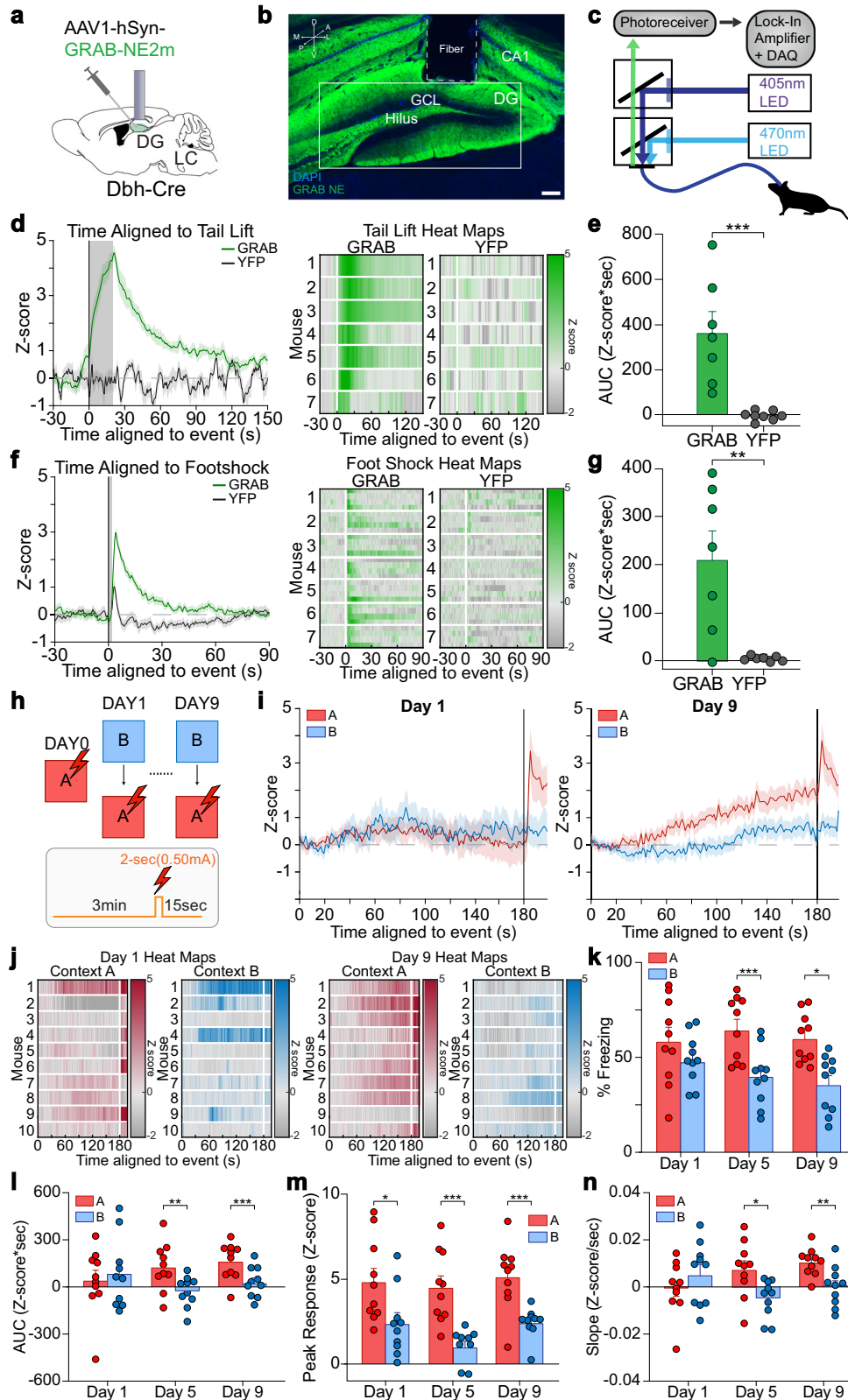
context B during days 5, 9, and 10, while there was no significant difference in AUC between the two contexts on days 1 and 11 (Supplementary Fig. 2h). In addition, we calculated the peak response between 180 and 197 s in each context, to quantify the response to foot shock in context A and saw significantly higher peak response in context A compared to context B on days 1, 5, and 9, indicating increased NE release in response to the aversive stimulus (Supplementary Fig. 2i).

There was also significantly increased peak response in context A compared to context B on day 10 but not on day 11, indicating the strength of the sustained NE release in context A compared to context B on day 10. We also calculated the slope of the NE dynamics, finding significant differences in slope between context A and context B during days 9 and 10 of training, but not days 1, 5, and 11 (Supplementary Fig. 2j). These results suggest that prolonged NE release in the DG

Fig. 1 | Linear elevations in tonic NE release within the DG occur during successful contextual discrimination of an aversive context. a Schematic of the experimental approach depicts infection of the dentate gyrus with GRAB$_{NE}$ and optical fiber implanted above the DG. **b** Representative image depicting expression of GRAB$_{NE}$ in DG driven by hSyn promoter and location of fiber implant ($n = 7$ mice). Scale bar = 100 μm. **c** Schematic of fiber photometry setup. **d** Averaged trace of GRAB$_{NE}$ and YFP control fluorescence (left) and individual heat maps of GRAB$_{NE}$ and YFP fluorescence for 20 s tail lift test (right). **e** Area under the curve analysis for GRAB$_{NE}$ and YFP control fluorescence for tail lift test ($n = 7$ mice). Unpaired two-tailed t test ($t_{(13)} = 4.35$, $p = 0.0008$). **f** Averaged trace of GRAB$_{NE}$ and YFP control (left) and individual heat maps of GRAB$_{NE}$ and YFP fluorescence for 2 s foot shock (right). **g** Area under the curve analysis for GRAB$_{NE}$ and YFP control fluorescence for 2 s foot shock ($n = 7$ mice). Unpaired two-tailed t-test

($t_{(13)} = 3.502$, $p = 0.0044$). **h** Schematic depicting CFD task. **i** Averaged traces of GRAB$_{NE}$ fluorescence during CFD training ($n = 10$ mice). **j** Individual heat maps during CFD training ($n = 10$ mice). **k** Freezing behavior during CFD training ($n = 10$ mice). Paired two-tailed t-test (Day 1: $t_{(9)} = 2.048$, $p = 0.0709$; Day 5: $t_{(9)} = 4.137$, $p = 0.0025$; Day 9: $t_{(9)} = 2.660$, $p = 0.0261$). **l** Area under the curve analysis of GRAB$_{NE}$ fluorescence levels during CFD training ($n = 10$ mice). Paired two-tailed t-test (Day 1: $t_{(9)} = 0.519$, $p = 0.6163$; Day 5: $t_{(9)} = 3.355$, $p = 0.0085$; Day 9: $t_{(9)} = 3.774$, $p = 0.0044$). **m** Peak response analysis of GRAB$_{NE}$ fluorescence levels during CFD training ($n = 10$ mice). Paired two-tailed t-test (Day 1: $t_{(9)} = 3.111$, $p = 0.0125$; Day 5: $t_{(9)} = 5.316$, $p = 0.0005$; Day 9: $t_{(9)} = 4.931$, $p = 0.0008$). **n** Average slope during CFD training ($n = 10$ mice). Paired two-tailed t test (Day 1: $t_{(9)} = 1.160$, $p = 0.2758$; Day 5: $t_{(9)} = 2.586$, $p = 0.0294$; Day 9: $t_{(9)} = 3.870$, $p = 0.0038$). All data are mean ± SEM. *$p < 0.05$, **$p < 0.01$, ***$p < 0.005$.

persists following contextual discrimination even in the absence of the aversive stimuli, and that the termination of this NE ramping occurs in association with the end of contextual learning.

Next, we aimed to elucidate potential differences in NE ramping due to repeated exposure to aversive stimuli and one extremely aversive stimulus. This was done through a modified CFD experiment that took place over two days, with increased foot shock intensity (Supplementary Fig. 3a, b). In this modified CFD task, mice successfully discriminated between context A and context B on the second day and displayed increased NE dynamics on day 2 in the unsafe context (Supplementary Fig. 3c–e). When these dynamics were quantified via an area under the curve (AUC) analysis, we observed a significantly increased amount of NE in context A compared to context B on day 2 during the first 180 seconds, as well as a significantly increased amount of NE in context A compared to context B in response to the foot shock (Supplementary Fig. 3f, g). We then used Pearson correlation to assess potential links between the difference in AUC and peak response in context A compared to context B with freezing ratio, finding that there were no significant correlations on day 1, but that there was a significant correlation between ΔAUC and freezing ration on day 9 (Supplementary Fig. 3h, i). Lastly, we calculated the slope of the NE dynamics, finding no significant differences in slope between context A and context B during either day of training (Supplementary Fig. 3j). These findings suggest similar NE dynamics in the DG during varying types of contextual fear learning.

Given that the hippocampus also likely receives dopamine as a byproduct of NE synthesis, it is possible that this neuromodulator may also be important in aversive contextual learning[34,35]. To this end, we repeated the CFD experiment with the novel biosensor GRAB$_{DA}$, a GPCR activation-based DA sensor with high specificity for DA, into the DG of DAT-cre mice (Supplementary Fig. 4a, b). On day 1 there were no significant differences in freezing in context A compared to context B, however on day 5 and day 9 there was a significantly increased amount of freezing in context A as compared to context B, indicating that mice successfully discriminated between the unsafe and safe contexts following training (Supplementary Fig. 4c). We also observed elevated dopamine signaling in both context A and context B by the end of the training, as well as elevated responses in response to the shock (Supplementary Fig. 4e–h). In addition, when we used Pearson correlation to assess potential links between the differences in AUC in context A compared to context B with freezing ratio, there were no significant correlations between these two factors (Supplementary Fig. 4i). There was however a significant correlation on day 9 when using Pearson correlation to assess potential links between the differences in peak response in context A compared to context B with freezing ratio (Supplementary Fig. 4j). Lastly, after calculating the slope of the DA dynamics, we found no significant differences between context A and context B during the early, middle, and late stages of training (Supplementary Fig. 4k). These results indicate that while DA is released in the DG during CFD, contextual discrimination as it relates to aversive content specifically is likely to not be mediated by DA in this paradigm.

However, the role of dopamine in CFD specifically requires substantial further evaluation, additional sensor selectivity types, and its own complete study.

Induction of elevations in DG NE dynamics is sufficient to cause contextual disambiguation in the absence of a salient aversive stimulus

Following the characterization of GRAB$_{NE}$ in the DG during endogenous NE release, we next characterized GRAB$_{NE}$ dynamics in response to evoked NE release. We injected GRAB$_{NE}$ into the DG and Cre-recombinase-dependent viral vectors containing the red-shifted light-sensitive cation channel ChrimsonR into the LC of Dbh-cre mice (Fig. 2a, b). We then implanted optical fibers above the DG for photometry recordings during contextual discrimination and began testing stimulation parameters to tune photo-stimulation to closely match endogenous NE dynamics seen in CFD (Fig. 2c). 20 Hz pulsed photo-stimulation for 20 s was delivered above the DG, during which we observed a significant increase in GRAB$_{NE}$ fluorescence during stimulation compared to YFP controls (Fig. 2d, e). This signal then decreased back to baseline following termination of the stimulation parameters. In a new series of experiments, we also delivered 1, 3, 5, and 10 Hz pulsed photostimulation for 20 s in separate trials and observed increasing levels of GRAB$_{NE}$ fluorescence with increasing levels of pulsed photostimulation of LC-DG terminals, suggesting that we are able to discreetly control the evoked release of NE from LC to DG (Fig. 2f–h). These results establish the successful characterization of GRAB$_{NE}$ for detecting spatiotemporal dynamics of evoked NE release from LC to DG, providing an optogenetic titration and calibration template for use in our contextual fear discrimination task.

We next examined how this increased and sustained release of NE in the aversive context during CFD would alter discrimination and recognition during contextual processing. To do this, we utilized GRAB$_{NE}$ with an optical fiber implanted in the DG and injected ChrimsonR into the LC of Dbh-cre mice (Fig. 2a, b). These mice underwent a modified CFD task, in which the foot shock was entirely replaced by a variable photo-stimulation of LC-DG terminals while in context A in order to closely match the NE linear ramping effects induced by shock (Fig. 2c, i). During the first 180 s of context A, mice received 1–5 Hz pulsed photostimulation, mimicking tonic NE release dynamics and resulting in sustained NE release over the session. Then, mice received 20–40 Hz pulsed photostimulation for 2 s, to replicate the phasic bursting we measured during responses to foot shock. The frequencies of stimulation that mice received were specifically calibrated for each individual mouse to mimic the endogenous NE peak response and dynamics measured during CFD, with stim matched ramping during the first 180 s and stim matched foot shock for 2 s in context A (Fig. 2j, k). Mice that underwent this modified CFD task displayed no differences in freezing between contexts in early or middle stages of training and displayed significantly increased freezing in context A compared to context B during the late stages of training, even in the absence of a salient aversive stimuli (Fig. 2l). To quantify the
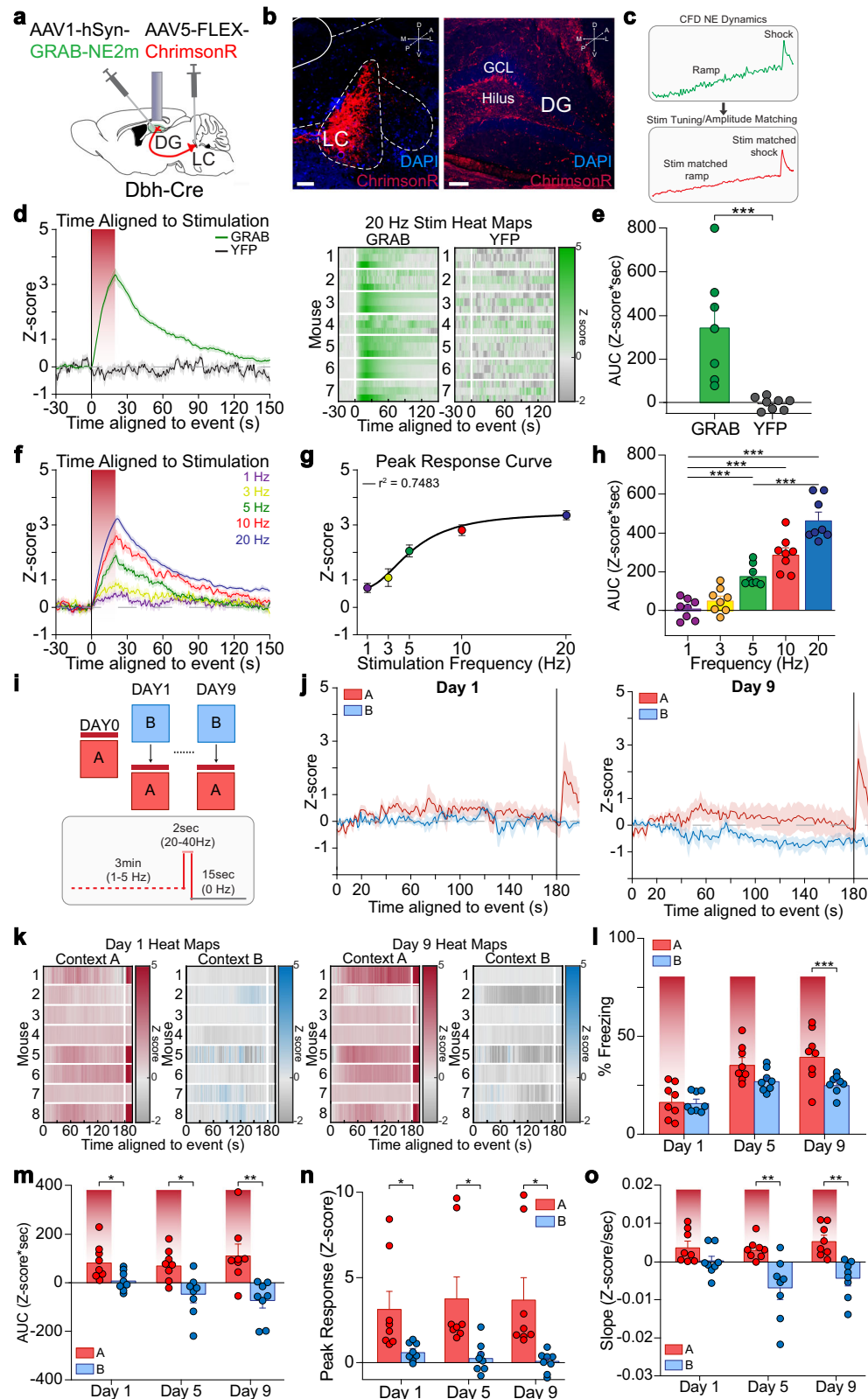
total amount of NE released in both context A and context B over time, an area under the curve (AUC) analysis was used, taking the AUC for each mouse in the first 180 s of both context A and context B. Stimulation occurred across each day of training, with significantly higher NE levels in the aversive context during early (day 1), middle (day 5) and late (day 9) stages of training, suggesting that the stimulation parameters chosen were sufficient to evoke prolonged NE release in the DG

in context A throughout the CFD task (Fig. 2m). These findings demonstrate increased learning over the course of the CFD task, in which mice show they are able to learn how to disambiguate between the two contexts by freezing more in context A, the "unsafe" context due to increased NE release, even in the absence of an aversive stimuli. To quantify whether there was a linear correlation between these two factors, we calculated a ratio between the proportion of freezing

Fig. 2 | Optogenetic control of linear elevations in DG NE dynamics is sufficient to cause contextual disambiguation in the absence of a salient aversive stimulus. a Schematic of the experimental approach depicts infection of DG with GRAB$_{NE}$, optical fiber implanted above the DG, and infection of LC with ChrimsonR. **b** Representative image depicting expression of ChrimsonR in LC (left) and terminal expression in DG (right) ($n = 7$ mice). Scale bar = 100 μm. **c** Stimulation tuning and amplitude matching for stimulation parameters compared to endogenous NE dynamics observed during CFD. **d** Averaged trace of GRAB$_{NE}$ and YFP control fluorescence (left) and individual heat maps of GRAB$_{NE}$ fluorescence for 20 Hz photostimulation for 20 s (right). **e** Area under the curve analysis for GRAB$_{NE}$ and YFP control fluorescence for 20 Hz photostimulation for 20 s ($n = 7$ mice). Unpaired two-tailed t-test ($t_{(13)} = 3.859$, $p = 0.002$). **f** Averaged traces of GRAB$_{NE}$ fluorescence for 1, 3, 5, 10, and 20 Hz photostimulation for 20 s. **g** Peak response curve for variable photostimulation ($n = 8$ mice). **h** Area under the curve analysis for GRAB$_{NE}$ fluorescence for variable photostimulation ($n = 8$ mice). Two-way ANOVA with Tukey's multiple comparisons (1 Hz vs. 3 Hz: $p = 0.7718$; 1 Hz vs. 5 Hz: $p = 0.0007$;

1 Hz vs. 10 Hz: $p < 0.0001$; 1 Hz vs. 20 Hz: $p < 0.0001$; 3 Hz vs. 5 Hz: $p = 0.0177$; 3 Hz vs. 10 Hz: $p < 0.0001$; 3 Hz vs. 20 Hz: $p < 0.0001$; 5 Hz vs. 10 Hz: $p = 0.0466$; 5 Hz vs. 20 Hz: $p < 0.0001$; 10 Hz vs. 20 Hz: $p = 0.0005$). **i** Schematic depicting CFD task. **j** Averaged traces of GRAB$_{NE}$ fluorescence during CFD training ($n = 8$ mice). **k** Individual heat maps during CFD training ($n = 8$ mice). **l** Freezing during CFD training ($n = 8$ mice). Paired two-tailed t test (Day 1: $t_{(7)} = 0.4134$, $p = 0.6917$; Day 5: $t_{(7)} = 1.998$, $p = 0.0859$; Day 9: $t_{(7)} = 4.184$, $p = 0.0041$). **m** Area under the curve analysis of GRAB$_{NE}$ fluorescence levels during CFD training ($n = 8$ mice). Paired two-tailed t test (Day 1: $t_{(7)} = 3.111$, $p = 0.0170$; Day 5: $t_{(7)} = 3.033$, $p = 0.0190$; Day 9: $t_{(7)} = 4.025$, $p = 0.005$). **n** Peak response analysis of GRAB$_{NE}$ fluorescence levels during CFD training ($n = 8$ mice). Paired two-tailed t-test (Day 1: $t_{(7)} = 2.390$, $p = 0.0482$; Day 5: $t_{(7)} = 2.446$, $p = 0.0443$; Day 9: $t_{(7)} = 3.260$, $p = 0.0139$). **o** Average slope during CFD training ($n = 8$ mice). Paired two-tailed t test (Day 1: $t_{(7)} = 1.538$, $p = 0.168$; Day 5: $t_{(7)} = 3.661$, $p = 0.0081$; Day 9: $t_{(7)} = 4.039$, $p = 0.0049$). All data are mean ± SEM. *$p < 0.05$, **$p < 0.01$, ***$p < 0.005$.

behavior in context A (unsafe) compared to context B (safe), and the change in AUC in context A (unsafe) compared to context B (safe). We then used linear regression and Pearson correlation to determine the relationship between these ratios for both the beginning and end of training (Supplementary Fig. 5a). While there is no significant relationship between the two variables at the beginning of training, by the end of the task there is a significant correlation between the freezing ratio and ΔAUC within the two contexts. This result indicates that mice receiving higher amounts of prolonged NE release in the "unsafe" context also performed better by the end of training in the CFD task, learning to disambiguate the two contexts in the absence of an aversive stimuli. In addition, we also quantified the peak response for each mouse in response to the foot shock in context A, with mice showing significantly increased NE release in context A compared to context B at 180 s when the foot shock was administered (Fig. 2n). In order to quantify a potential relationship between freezing and peak response, we use a Pearson correlation analysis between the difference in peak response in context A vs. context B and the freezing differences in context A vs. context B (Supplementary Fig. 5b). Here, no significant correlation was found between freezing and peak response in both the beginning and end of training. Furthermore, we calculated the slope of the NE dynamics, finding significant differences in slope between context A and context B during the middle and end stages of training, but not the beginning (Fig. 2o). During this modified contextual fear paradigm with stimulation matching, in context B, we noticed a decaying signal that was not seen prior. We hypothesized that this decay was due to a lack of salient stimuli during this altered CFD paradigm. Therefore, we conducted another altered CFD experiment in which mice were placed in both context A and B for 197 s with no salient stimuli or stimulation (Supplementary Fig. 5c, d). Mice that received no stimulation in either of the two contexts displayed no significant differences in freezing, AUC, slope, and correlation between the freezing ratio and ΔAUC over the course of training (Supplementary Fig. 5e–j).Taken together, these results indicate that mice experience increased discrimination between two contexts when NE is increased in a linear manner within the DG in one context, in the absence of salient aversive stimuli such as foot shock, and that the stronger the tonic elevation in NE release is over the trial, the better the performance of disambiguating both contexts in the CFD task.

Mimicking endogenous ramping of NE tonic release in the DG is sufficient for contextual disambiguation in the absence of a salient aversive stimulus

We next aimed to isolate the specific spatiotemporal NE release dynamics responsible for causing discrimination between two contexts in the absence of salient stimuli. In order to do this, we again utilized GRAB$_{NE}$ with an optical fiber implanted in the DG, and injected ChrimsonR into the LC of Dbh-cre mice for use in fiber photometry

(Fig. 3a). We again used a modified CFD task, during which we reproduced the NE release event in response to a foot shock by delivering 20–40 Hz pulsed photostimulation for 2 s after 180 s in context A (Fig. 3b, c). Here, we were again able to effectively calibrate stimulation to mimic endogenous NE dynamics measured during the foot shock delivered during CFD with stimulation-matched shock (Fig. 3d, e). When these mice were stimulated to reproduce a foot shock NE release event during CFD, across each day of training, we observed no significant differences in freezing between the two contexts (Fig. 3f). These mice also displayed no differences in AUC during the first 180 s of training, suggesting no endogenous prolonged NE release was occurring (Fig. 3g) due to the accumulation of foot-shock release events as the trial unfolded. We again calculated the ratio between the proportion of freezing behavior in context A (unsafe) compared to context B (safe), and the change in AUC in context A (unsafe) compared to context B (safe). We used linear regression and Pearson correlation to assess the relationship between these ratios for both the beginning and end of training. In this case, no correlative relationship was observed between the freezing ratio and ΔAUC in mice that received only 2 s of 20–40 Hz pulsed photostimulation throughout training (Supplementary Fig. 6a, b). In addition, we also quantified the peak NE release response in each mouse due to high-frequency stimulation in context A, with mice showing significantly increased NE release in context A compared to context B at 180 s (Fig. 3h). In order to quantify a potential relationship between freezing and peak response, we used a Pearson correlation between the difference in peak response in context A vs. context B and the freezing differences in context A vs. context B (Supplementary Fig. 6c). No significant correlation was found between freezing and peak response at both the beginning and end of training. We again calculated the slope of the NE dynamics, finding no significant differences in slope between context A and context B during the CFD task (Fig. 3i).

Next, we used another modified CFD task, in which the prolonged NE release was mimicked by variable stimulation of LC-DG terminals while in context A to match stimulation to endogenous NE dynamics during CFD (Fig. 3j–l). In this case, we delivered only 1–5 Hz pulsed photostimulation for 180 s, without the 2 s of high-frequency stimulation afterward, to mimic only the prolonged NE release seen in context A during CFD. This resulted in prolonged tonic NE release dynamics similar to those originally observed during the traditional CFD paradigm (Fig. 3m, n). During this modified CFD paradigm with stimulation-matched ramping, mice showed significantly increased freezing in context A compared to context B on day 9 of the CFD task, while no differences in freezing were observed on day 1 or day 5 of the task (Fig. 3o). To quantify the amount of NE released in both context A and context B, an area under the curve (AUC) analysis was used, taking the AUC for each mouse in the first 180 s of both context A and context B. Stimulation occurred across each day of training, only in context A,
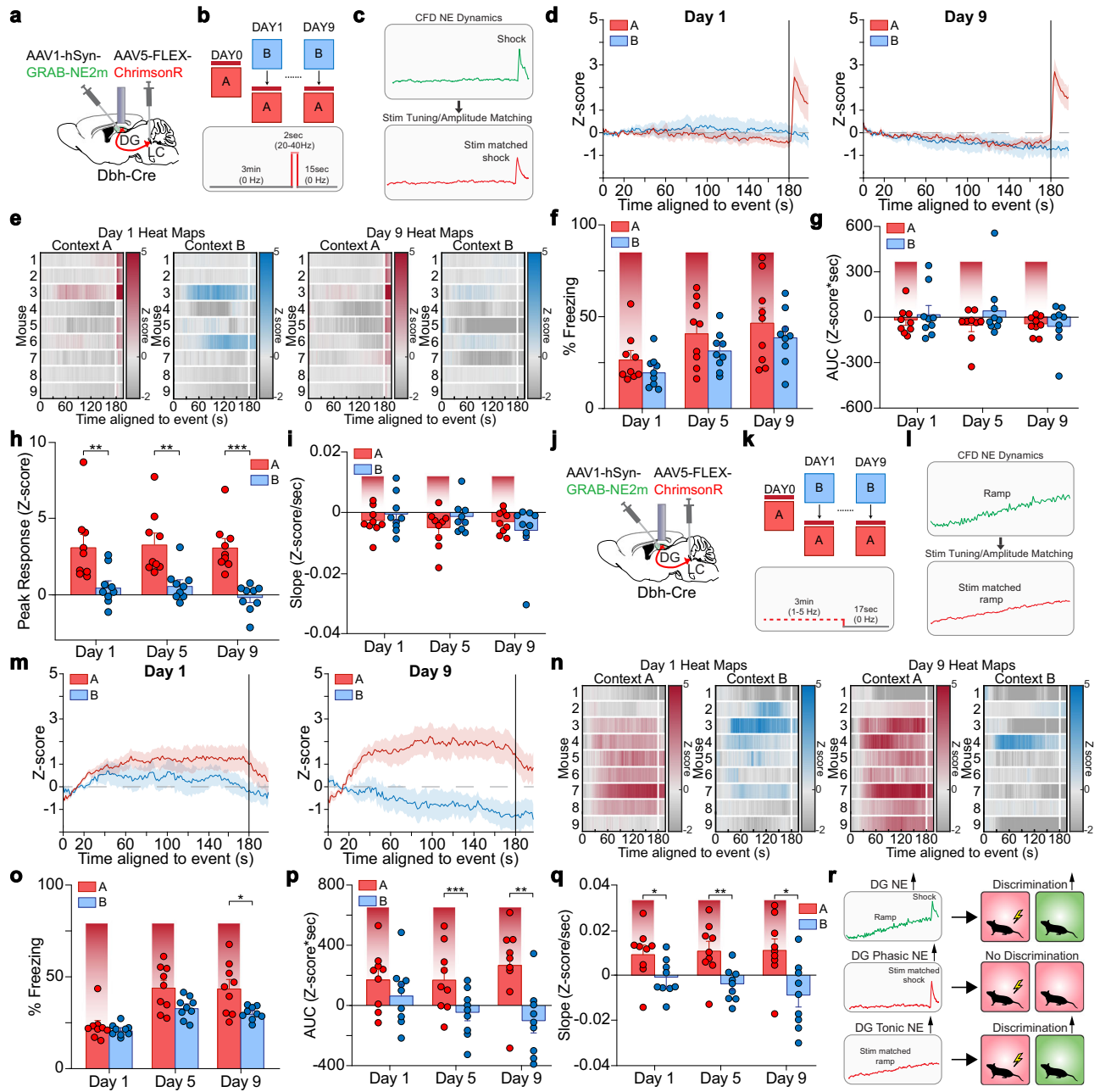
Fig. 3 | Mimicking endogenous ramping of NE tonic release in the DG is sufficient for contextual disambiguation in the absence of a salient aversive stimulus. a Schematic of the experimental approach depicts infection of DG with GRAB$_{NE}$, optical fiber implanted above the DG, and infection of LC with ChrimsonR. **b** Schematic depicting CFD task. **c** Stimulation tuning and amplitude matching for stimulation parameters compared to endogenous NE dynamics observed during CFD. **d** Averaged traces of GRAB$_{NE}$ fluorescence during CFD training ($n = 9$ mice). **e** Individual heat maps during CFD training ($n = 9$ mice). **f** Freezing behavior during CFD training ($n = 9$ mice). Paired two-tailed t test (Day 1: $t_{(8)} = 1.480$, $p = 0.1773$; Day 5: $t_{(8)} = 1.114$, $p = 0.2975$; Day 9: $t_{(8)} = 0.9306$, $p = 0.3793$). **g** Area under the curve analysis of GRAB$_{NE}$ fluorescence levels during CFD training ($n = 9$ mice). Paired two-tailed t test (Day 1: $t_{(8)} = 1.344$, $p = 0.2158$; Day 5: $t_{(8)} = 1.090$, $p = 0.3074$; Day 9: $t_{(8)} = 0.4070$, $p = 0.6947$). **h** Peak response analysis of GRAB$_{NE}$ fluorescence levels during CFD training ($n = 9$ mice). Paired two-tailed t test (Day 1: $t_{(8)} = 4.519$, $p = 0.0020$; Day 5: $t_{(8)} = 3.535$, $p = 0.0077$; Day 9: $t_{(8)} = 5.824$, $p = 0.0004$). **i** Average slope during CFD training ($n = 9$ mice). Paired two-tailed t test (Day 1: $t_{(8)} = 1.380$,

$p = 0.2051$; Day 5: $t_{(8)} = 1.085$, $p = 0.3097$; Day 9: $t_{(8)} = 0.8658$, $p = 0.4118$). **j** Schematic of experimental approach depicts infection of DG with GRAB$_{NE}$, optical fiber implanted above the DG, and infection of LC with ChrimsonR. **k** Schematic depicting CFD task. **l** Stimulation tuning and amplitude matching for stimulation parameters compared to endogenous NE dynamics observed during CFD. **m** Averaged traces of GRAB$_{NE}$ fluorescence during CFD training ($n = 9$ mice). **n** Individual heat maps during CFD training ($n = 9$ mice). **o** Freezing behavior during CFD training ($n = 9$ mice). Paired two-tailed t test (Day 1: $t_{(8)} = 0.9955$, $p = 0.3486$; Day 5: $t_{(8)} = 2.072$, $p = 0.0720$; Day 9: $t_{(8)} = 2.735$, $p = 0.0257$). **p** Area under the curve analysis of GRAB$_{NE}$ fluorescence levels during CFD training ($n = 9$ mice). Paired two-tailed t test (Day 1: $t_{(8)} = 1.335$, $p = 0.2187$; Day 5: $t_{(8)} = 5.359$, $p = 0.0007$; Day 9: $t_{(8)} = 3.611$, $p = 0.0069$). **q** Average slope during CFD training ($n = 9$ mice). Paired two-tailed t-test (Day 1: $t_{(8)} = 3.197$, $p = 0.0127$; Day 5: $t_{(8)} = 4.235$, $p = 0.0029$; Day 9: $t_{(8)} = 3.053$, $p = 0.0157$). **r** Schematic depicting major findings that elevation of NE tonic release in the DG is sufficient for contextual disambiguation in the absence of a salient aversive stimulus. All data are mean ± SEM. *$p < 0.05$, **$p < 0.01$, ***$p < 0.005$.

leading to significantly increased NE levels in context A compared to context B across the middle and late stages of training (Fig. 3p). These findings indicate that over the course of training, mice were able to discriminate successfully between context A and context B via the presence of prolonged elevated tonic NE release in context A, even in the absence of a salient aversive stimuli or a foot shock-like evoked phasic NE response. We next calculated a ratio between the proportion of freezing behavior in context A (unsafe) compared to context B (safe), and the change in AUC in context A (unsafe) compared to context B (safe). We used linear regression and Pearson correlation to assess the relationship between these ratios for both the beginning and end of training (Supplementary Fig. 6d, e). While no significant relationship between the two variables was observed at the beginning of training, by the end of the task, there was a significant correlation between the freezing ratio and ΔAUC in the two contexts. When we calculated the slope of the NE dynamics, we found significant differences in slope between context A and context B during the beginning, middle and end stages of training (Fig. 3q). These results indicate that linear elevations in tonic NE release within the DG in response to contextual cues are a critical driving force behind contextual discrimination of a safe versus unsafe context (Fig. 3r). In addition, our data suggest that a single robust phasic burst release of NE within the DG as related to the aversive stimuli is not sufficient to produce robust contextual discrimination in response to aversive stimuli. Taken together, these results establish a critical role for linear tonic increases (ramps) of NE release in the DG as crucial for promoting contextual discrimination.

Discussion

In the current study, we report that a particular pattern of linear ramping of LC-NE release into the DG results in successful contextual discrimination between a safe and unsafe context in an aversive contextual discrimination task. This is likely through elevated LC-NE neuron tonic firing in response to environmental cues[36]. We observe sustained ramping of NE release in an aversive context during successful contextual disambiguation in an aversive fear discrimination task and we were able to cause contextual disambiguation using optogenetic mimicry of evoked NE release temporal dynamics. These results further establish the noradrenergic DG interactions as critical for differentiating between new and previous events and indicate that responses to contextual differences are determined by the incoming spatiotemporal dynamics of NE release during an aversive experience.

Previous work has implicated prolonged phasic dopamine signals in the striatum as important in signaling proximity and value of reward[37]. In this study, it was postulated that ramping dopamine signals may provide a continuous estimate of the distance and size of the reward and maintain motivation toward that reward. In addition, further work implicates burst stimulation of ventral tegmental area (VTA) neurons in causing a prolonged increase of dopamine in the nucleus accumbens and prefrontal cortex[38]. Here however, we demonstrate prolonged ramping norepinephrine release in response to contextual discrimination, in which this NE ramping occurs in the time leading up to delivery of a salient aversive foot shock in the CFD task, during which the animal must rely on contextual cues to disambiguate the unsafe (shock) and safe (no shock) contexts (Fig. 1). In addition, while in prior studies of monoamine ramping the prolonged increases in tone occurred for up to 10 s, the NE ramping we report here is exciting because it is quite sustained, lasting for 180 s prior to the foot shock stimuli. This suggests that there is an extended time scale function for ramping NE release within the DG, especially during pattern separation, where continuous processing on contextual clues may be necessary for successful discrimination to occur. In addition, we demonstrated prolonged ramping dopamine release in both contexts during contextual discrimination, suggesting a potential role for ramping dopamine during contextual fear learning as well

(Supplementary Fig. 4). However, because the ramping takes place in both contexts, this signal appears to be unique from the ramping norepinephrine observed. It is possible that dopamine ramping is responsible for spatial processing, rather than contextual discrimination. Further investigations are needed to more clearly understand how these prolonged neurotransmitter dynamics are mechanistically involved in contextual learning. For example, whether these prolonged ramps of NE release are involved in specific phases of memory such as encoding, consolidation, or extinction. Our results suggest that it will be important to further study the specific methods by which dopamine and norepinephrine regulate contextual discrimination through reuptake, receptor-selective binding, and signaling, and to better isolate the roles of these neurotransmitters in DG function[39].

In this study, we opted to use both male and female mice in the CFD task. Existing literature supports potential sex differences in aversive contextual processing in both rodents and humans, with females more likely to present with symptoms and be diagnosed with PTSD[40]. In addition, female rats outperformed male rats in a contextual fear discrimination task, while male rats outperformed female rats in a Morris water maze spatial learning task[41,42]. However, in our CFD task, no differences in contextual discrimination performance were observed between male and female mice (Supplementary Fig. 1l). This may be due to differences in the contextual fear conditioning procedure used, as well as differences in the difficulty of the CFD task. Because sex is a prominent risk factor for the development of PTSD in human trauma-exposed adults, further understanding of the potential sex differences in LC-DG mediated pattern separation may be important in the development of therapeutic strategies for the treatment of PTSD and PTSD-like symptoms[43,44].

Throughout this study, we opted to continue the use of an established contextual fear conditioning paradigm, as demonstrated in other previous work[12,17,32]. In this CFD task, animals undergo 9 days of training in which context B is presented before context A. In our testing, when context A and B presentations were alternated, this created a task that was difficult to the point that mice were unable to successfully discriminate between the safe and unsafe contexts[17]. Thus, maintaining the same order of contextual presentation is necessary to create a baseline in which the animals are able to discriminate between the contexts so that norepinephrine signaling can be observed during this successful discrimination. Furthermore, during this task we opted to continue the use of cinnamon and peppermint as odorants for the unsafe and safe contexts, respectively. While peppermint odor has been shown to be aversive at higher concentrations, this would not affect our experimental findings, as we used a low dose of peppermint odor in the safe context, while mice showed higher freezing levels in the unsafe context, which contained cinnamon odor instead. In addition, when mice underwent a modified CFD experiment in which they did not receive a shock in either context, there were no significant differences in freezing between context A and context B, indicating no bias towards either odor in the absence of an aversive stimuli (Supplementary Fig. 5). Therefore, the discrepancy in freezing levels is not due to the use of a potentially aversive odorant or bias toward a specific odor.

We also conducted several modified CFD experiments in this work, including an extinction paradigm and a shortened, heightened aversion paradigm (Supplementary Figs. 2 and 3). During the extinction paradigm, we observed prolonged NE release in context A on day 10, even without the presentation of the foot shock, with this prolonged release remaining elevated throughout the entirety of the 15-minute trial. This was accompanied by increased freezing in context A compared to context B. However, on day 11, this ramping no longer took place, and the animals learned to disassociate context A from the foot shock, as there were no significant differences in freezing between context A and context B. These findings further support that as mice undergo contextual learning, there is a corresponding change in

prolonged NE dynamics in the DG to inform their behavior. Meanwhile, with the shortened 2-day CFD task, we aimed to understand potential differences in NE dynamics in response to one extremely salient stimulus, as opposed to repeated exposures. In this case, we found that animals do still undergo NE ramping in context A following successful learning of the CFD task, although the change was not as pronounced as during our standard 10-day CFD task. This experiment suggests that similar but not identical mechanisms exist for varying types of contextual learning, which could help inform our treatment of those suffering from PTSD, as there may be differences in the development of PTSD following repeated exposure to traumatic events compared to exposure to a singular highly traumatic event. Thus, further research must be done regarding the mechanisms by which norepinephrine regulates contextual discrimination and to better isolate the roles of norepinephrine in DG function.

In addition, during the modified CFD task used here wherein mice received one of the four different stimulation parameters, there appeared to be gradual decreases in NE tone (quantified by AUC analysis) over the course of training in context B, where no stimulation occurred (Figs. 2, 3 and Supplementary Fig. 5). This is likely due to the established role for LC-NE in novelty encoding as well as contextual learning[45,46]. We postulate that during this contextual fear discrimination task, and in the absence of aversive stimuli, mice undergo increased NE release in both contexts during the initial stages of training, as they experience these novel contexts for the first time. However, as these mice become habituated to the contexts, and without any salient cues to respond to, this novelty encoding likely decreases, leading to decreased amounts of NE in the DG during the CFD task, which is then overcome in context A via increased evoked NE release due to photostimulation of LC-DG terminals. There also appear to be high variances in basal anxiety states between distinct cohorts of mice, as seen in the freezing levels during the initial stages of contextual fear discrimination. This is known in the field, and we do our best to control for these differences with animal handling and reverse light cycle housing. However, these variances were also observed in our previous efforts using this discrimination task, and differences in initial freezing during the first day of training do not appear to impact overall performance in the task by the end of training[17].

Overall, our findings presented here provide us with a better understanding of the spatiotemporal properties of norepinephrine release and its time-locked receptor-mediated signaling actions during aversive contextual discrimination. We demonstrated here that increases in tonic ramping of NE release occur within the DG during successful contextual discrimination. In addition, mimicking this ramping effect through photoactivation of LC-DG terminals is sufficient to drive pattern separation and contextual disambiguation in the CFD task, even in the absence of salient aversive stimuli such as foot shock resolving when, where, and how NE release in the hippocampus, specifically the DG, influences behavior. Understanding the spatiotemporal mechanisms by which monoamine neuromodulators coordinate aversive processing will aide in the development of novel therapeutic strategies for targeting psychiatric disorders characterized by generalization, including PTSD and anxiety.

Methods

Animals
Adult (20–35 g) male and female *Dbh*-Cre mice, *DAT*-IRES-cre mice, and Cre (-) littermate control mice were used for projection mapping and all in vivo experiments after backcrossing to C57BL/6J mice for at least 10 generations. Mice were group housed, given access to food pellets and water *ad libitum*, and maintained on a 12:12-h reverse light/dark cycle (lights on at 8:00 p.m.). The mice were bred at the University of Washington. Animals were held in a sound attenuated holding room facility in the lab starting at least one week prior to surgery, as well as post-surgery and throughout the duration of behavioral assays to minimize stress from transportation and disruption from foot traffic. All mice were handled and, where appropriate, connected to fiber optics two times a day for one week prior to behavioral experimental testing. All experimental procedures were approved by the Animal Care and Use Committee of the University of Washington and conformed to UW National Institutes of Health guidelines.

Stereotaxic surgery
After acclimatizing to the holding facility for 7–9 days, the animals were anesthetized in an induction chamber (4% isoflurane, Piramal Healthcare, Maharashtra, India) and mounted on a stereotaxic frame under sterile conditions (Kopf Instruments, Model 1900) where they were maintained at 1–2% isoflurane for the duration of the surgery. For in vivo fiber photometry experiments, adult mice were injected bilaterally with 800 nl in each side of AAV5/Syn-FLEX-ChrimsonR-td-Tomato (Addgene) into the LC (AP: − 5.45 mm, ML: ±1.25 mm, DV: − 3.8 mm) using a Hamilton syringe with a beveled needle and injected unilaterally with 400 nl of AAV1-hsyn-GRAB-NE2m or AAV9-hsyn-GRAB-DA2m (Yulong Li Lab) into the DG (AP: − 2.15 mm, ML: + 1.4 mm, DV: − 2.1 mm) using a Hamilton syringe with a blunted needle. Transgenic controls were injected bilaterally with 800 nl of AAV5/Syn-FLEX-ChrimsonR-td-Tomato into the LC (AP: − 5.45 mm, ML: ±1.25 mm, DV: − 3.8 mm) using a Hamilton syringe with a beveled needle and injected unilaterally with 400 nl of AAV5-Ef1a-DIO-EYFP (Addgene) into the DG using a Hamilton syringe with a blunted needle. Mice then received intracranial fiber photometry implants in the DG (AP: − 2.15 mm, ML: + 1.4 mm, DV: − 1.7 mm), which were secured using MetaBond (C & B Metabond). Mice were allowed to recover for at least six weeks following infusion of virus and intracranial implant prior to further behavioral testing or perfusion for projection mapping to ensure optimal viral expression. Mice were perfused at the conclusion of behavior to ensure optimal viral expression and optical implant placement location (Supplementary Fig. 6f).

Tissue collection and immunohistochemistry
After the conclusion of behavioral testing, mice were anesthetized with sodium pentobarbital and transcardially perfused with ice-cold PBS, followed by 4% phosphate-buffered paraformaldehyde. Brains were removed, postfixed overnight in 4% paraformaldehyde, and then saturated in 30% phosphate-buffered sucrose for 2–4 days at 4 °C. Brains were sectioned at 30 mM on a microtome and stored in a 0.01 M phosphate buffer at 4 °C prior to immunohistochemistry and tracing experiments. For behavioral cohorts, viral expression and optical fiber placements were confirmed before inclusion in the presented datasets. Viral expression and implant placements were verified using fluorescence and confocal (Leica Microsystems) microscopy. Images were produced with 10X, 20X, and 63X objectives and analyzed using ImageJ software (NIH) and Leica Application Suite Advanced Fluorescence software.

Fear conditioning
Fear conditioning took place in Med-Associates conditioning chambers that consisted of one clear plexiglass wall, three aluminum walls, and a stainless-steel grid as a floor. The training chamber was housed in a sound-attenuated cubicle. The conditioning chambers could be configured into two distinct contexts: A and B. Context A was rectangular, with floors made of stainless-steel rods (2 mm diameter, spaced 5 mm apart), walls of aluminum and acrylic, and cinnamon extract scent, and was cleaned with 70% ethanol between runs. Context B differed from context A in that it had a white acrylic floor, and a wall decorated with a black and white striped pattern. Context B was cleaned with multi-purpose surface cleaner (Method, UPC: 817939000106) between runs, and scented with peppermint extract. All sessions were recorded from the side using a digital camera and were scored for freezing by an investigator blinded to the genotype and experimental conditions of the animal.

For in vivo fiber photometry during behavior tests, a rotating optical commutator (Doric) was positioned on top of the training chamber and connected to a fiber photometry recording rig (Thorlabs). Fibers were attached to the implants on the mouse for every training session.

Contextual fear discrimination (CFD)

Mice were handled for 5 min per day for a week prior to training. Contextual fear discrimination training took place in the apparatus described above. During a standard CFD experiment, in context A (unsafe context), animals were placed in the conditioning chamber and allowed to freely explore for 180 s, after which they received a single 2 s foot shock of 0.50 mA. Mice were taken out 15 seconds after the termination of the foot shock and returned to their home cage. In context B (safe context), mice were allowed to freely explore the context for 197 seconds, the same amount of total time that they were in context A, and then returned to their home cage. In this context, no foot shock was delivered. On the first day (Day 0) of CFD training, animals were placed in context A and received a foot shock. The next day (Day 1), mice were run first in context B with no foot shock, then in context A with a foot shock. There was a minimum 3-hour period between exposure to context A and context B. This training protocol was repeated daily for 9 days. All freezing in both contexts was assessed for the first 180 s, and the last 17 s were not included in the behavioral analysis. Freezing was done manually by an investigator in a double-blind fashion to avoid bias in scoring. Mice only underwent one CFD experiment.

For the modified extinction CFD experiment, mice followed the standard CFD experiment described above through day 9 (Supplementary Fig. 2). Then, on days 10 and 11, mice were placed into the conditioning chamber and allowed to freely explore for 15 min, after which they were taken out and returned to their home cage. They were run first in context B with no foot shock and then in context A with no foot shock. There was a minimum 3-hour period between exposure to context A and context B.

For the modified two-day CFD experiment, mice followed the standard CFD experiment described above for only two days, day 1 and day 2 (Supplementary Fig. 3). During these days, in context A (unsafe context), animals were placed in the conditioning chamber and allowed to freely explore for 180 s, after which they received a single 2 s foot shock of 1 mA. Mice were taken out 15 seconds after the termination of the foot shock and returned to their home cage. In context B (safe context), mice were allowed to freely explore the context for 197 seconds, the same amount of total time that they were in context A, and then returned to their home cage.

For the modified CFD experiments using stimulation in place of salient stimuli, mice placed in context A (unsafe context) were allowed to freely explore for 197 s and received one of four stimulation parameters: low frequency (1–5 Hz) stimulation for 180 s, followed by high frequency (20–40 Hz) stimulation for 2 s, followed by no stimulation for 15 s; low frequency (1–5 Hz) stimulation for 180 s followed by no stimulation for 17 s; no stimulation for 180 s, followed by high frequency (20–40 Hz) stimulation for 2 s, followed by no stimulation for 15 s; no stimulation for 197 s. Mice were removed from the conditioning chamber after termination of the stimulation parameters and returned to their home cage. Stimulation frequencies were calibrated for each individual mouse based on fit to endogenous NE release dynamics in the CFD task during successful contextual discrimination (Fig. 1). These frequencies were tested for each mouse prior to the CFD task in a separate, neutral context.

In vivo fiber photometry

Fiber photometry recordings were made throughout the entirety of the CFD training sessions. Prior to recording, an optical fiber was attached to the implanted fiber using a ferrule sleeve (Doric, ZR_2.5).

Two LEDs were used to excite $GRAB_{NE}$ and $GRAB_{DA}$. A 531 Hz sinusoidal LED light (Thorlabs, LED light: M470F3; LED driver: DC4104) was bandpass filtered (470 ± 20 nm, Doric, FMC4) to excite $GRAB_{NE}$/$GRAB_{DA}$ and evoke NE/DA-dependent emission. A 211 Hz sinusoidal LED light (Thorlabs, LED light: M405FP1; LED driver: DC4104) was bandpass filtered (405 ± 10 nm, Doric, FMC4) to excite $GRAB_{NE}$/$GRAB_{DA}$ and evoke NE/DA-independent isosbestic control emission. Prior to recording, a 300 s period of $GRAB_{NE}$/$GRAB_{DA}$ excitation with 405 nm and 470 nm light was used to remove the majority of baseline drift. Laser intensity for the 470 nm and 405 nm wavelength bands were measured at the tip of the optical fiber and adjusted to ~ 50 µW before each day of recording. $GRAB_{NE}$/$GRAB_{DA}$ fluorescence traveled through the same optical fiber before being bandpass filtered (525 ± 25 nm, Doric, FMC4), transduced by a femtowatt silicon photoreceiver (Newport, 2151) and recorded by a real-time processor (TDT, RZ5P). The envelopes of the 531 Hz and 211 Hz signals were extracted in real time by the TDT program Synapse at a sampling rate of 1017.25 Hz. Optogenetic stimulation was delivered using a 625 nm sinusoidal LED light (Thorlabs, LED light: M625F2; LED driver DC4104) to excite LC-DG terminals expression ChrimsonR.

Photometry analysis

Custom MATLAB scripts were developed for analyzing fiber photometry data in the context of mouse behavior and can be accessed via GitHub (https://github.com/Bruchas-Lab). The isosbestic 405 nm excitation control signal was subtracted from the 470 nm excitation signal to remove movement artifacts from intracellular NE-dependent $GRAB_{NE}$/$GRAB_{DA}$ fluorescence. Baseline drift was evident in the signal due to slow photobleaching artifacts, particularly during the first several minutes of each hour-long recording session. A double exponential curve was fit to the raw trace and subtracted to correct for baseline drift. After baseline correction, the photometry trace was z-scored relative to the mean and standard deviation of the test session. The post-processed fiber photometry signal was analyzed in the context of animal behavior during the contextual fear discrimination task.

Quantification of NE release was obtained using the trapz function in conjunction with custom MATLAB scripts. This function utilizes numerical integration using the trapezoidal method, which approximates integration by breaking the area down into trapezoids with more easily computable areas. For an integration with $N + 1$ evenly spaced points, the approximation is:

$$\int_a^b f(x)dx \approx \frac{b-a}{2N}\sum_{n=1}^{N}(f(x_n)+f(x_{n+1}))$$
$$= \frac{b-a}{2N}\left[f(x_1)+2f(x_2)+...+2f(x_N)+f(x_{N+1})\right]$$

Quantification and statistical analysis

All data are expressed as mean ± SEM. Behavioral data were analyzed with GraphPad Prism 10.0 (GraphPad, La Jolla, CA). Two-tailed *student's t* test, one-way or two-way ANOVAs were used to analyze between-subjects designs. Repeated-measures designs were analyzed using a mixed-effects restricted maximum likelihood (REML) model. Tukey was used for *post-hoc* pairwise comparisons. The null hypothesis was rejected at the $p < 0.05$ level. Statistical significance was taken as $*p < 0.05$, $**p < 0.01$, $***p < 0.005$, *n.s.* represents not significant. All statistical information is listed in Supplementary Table 1.

Reporting summary

Further information on research design is available in the Nature Portfolio Reporting Summary linked to this article.

Data availability

Data generated or analyzed during this study are included in this published article as Source Data. Source data are provided in this paper.

Code availability

Custom MATLAB analysis code was created to appropriately organize, process, and combine fiber photometry data with associated behavioral data. Analysis code for photometry from Figs. 1–3, and Supplementary Figs. 1–5 will be made available online at https://www.github.com/Bruchas-Lab.

References

1. Liberzon, I. & Abelson, J. L. Context processing and the neurobiology of post-traumatic stress disorder. *Neuron* **92**, 14–30 (2016).
2. Lisman, J. E. et al. Circuit-based framework for understanding neurotransmitter and risk gene interactions in schizophrenia. *Trends Neurosci.* **31**, 234–242 (2008).
3. Shohamy, D. et al. Learning and generalization in schizophrenia: effects of disease and antipsychotic drug treatment. *Biol. Psychiatry* **67**, 926–932 (2010).
4. Kheirbek, M. A., Klemenhagen, K. C., Sahay, A. & Hen, R. Neurogenesis and generalization: a new approach to stratify and treat anxiety disorders. *Nat. Neurosci.* **15**, 1613–1620 (2012).
5. Besnard, A. & Sahay, A. Adult hippocampal neurogenesis, fear generalization, and stress. *Neuropsychopharmacology* **41**, 24–44 (2016).
6. Siegmund, A. & Wotjak, C. T. Toward an animal model of post-traumatic stress disorder. *Ann. N. Y. Acad. Sci.* **1071**, 324–334 (2006).
7. Raskind, M. A. et al. Reduction of nightmares and other PTSD symptoms in combat veterans by prazosin: a placebo-controlled study. *Am. J. Psychiatry* **160**, 371–373 (2003).
8. Taylor, H. R., Freeman, M. K. & Cates, M. E. Prazosin for treatment of nightmares related to posttraumatic stress disorder. *Am. J. Health Syst. Pharm.* **65**, 716–722 (2008).
9. Danielson, N. B. et al. Distinct contribution of adult-born hippocampal granule cells to context encoding. *Neuron* **90**, 101–112 (2016).
10. Deng, W., Mayford, M. & Gage, F. H. Selection of distinct populations of dentate granule cells in response to inputs as a mechanism for pattern separation in mice. *Elife* **2**, e00312 (2013).
11. Lisman, J. et al. Viewpoints: how the hippocampus contributes to memory, navigation and cognition. *Nat. Neurosci.* **20**, 1434–1447 (2017).
12. McHugh, T. J. et al. Dentate gyrus NMDA receptors mediate rapid pattern separation in the hippocampal network. *Science* **317**, 94–99 (2007).
13. Woods, N. I. et al. The dentate gyrus classifies cortical representations of learned stimuli. *Neuron* **107**, 173–184 (2020).
14. Marr, D. Simple memory: a theory for archicortex. *Philos. Trans. R. Soc. Lond. B Biol. Sci.* **262**, 23–81 (1971).
15. Morris, R. G. Elements of a neurobiological theory of hippocampal function: the role of synaptic plasticity, synaptic tagging and schemas. *Eur. J. Neurosci.* **23**, 2829–2846 (2006).
16. O'Reilly, R. C. & McClelland, J. L. Hippocampal conjunctive encoding, storage, and recall: avoiding a trade-off. *Hippocampus* **4**, 661–682 (1994).
17. Seo, D. O. et al. A locus coeruleus to dentate gyrus noradrenergic circuit modulates aversive contextual processing. *Neuron* **109**, 2116–2130 (2021).
18. Britton, K. T., Segal, D. S., Kuczenski, R. & Hauger, R. Dissociation between in vivo hippocampal norepinephrine response and behavioral/neuroendocrine responses to noise stress in rats. *Brain Res.* **574**, 125–130 (1992).
19. Campeau, S. et al. Stress rapidly increases alpha 1d adrenergic receptor mRNA in the rat dentate gyrus. *Brain Res.* **1323**, 109–118 (2010).
20. Fa, M. et al. Stress modulation of hippocampal activity–spotlight on the dentate gyrus. *Neurobiol. Learn Mem.* **112**, 53–60 (2014).
21. Blackstad, T. W., Fuxe, K. & Hökfelt, T. Noradrenaline nerve terminals in the hippocampal region of the rat and the guinea pig. *Z. Zellforsch. Mikros. Anat.* **78**, 463–473 (1967).
22. Ungerstedt, U. Stereotaxic mapping of the monoamine pathways in the rat brain. *Acta Physiol. Scand. Suppl.* **367**, 1–48 (1971).
23. McCall, J. G. et al. CRH engagement of the locus coeruleus noradrenergic system mediates stress-induced anxiety. *Neuron* **87**, 605–620 (2015).
24. McCall, J. G. et al. Locus coeruleus to basolateral amygdala noradrenergic projections promote anxiety-like behavior. *Elife* **6**, e18247 (2017).
25. Uematsu, A. et al. Modular organization of the brainstem noradrenaline system coordinates opposing learning states. *Nat. Neurosci.* **20**, 1602–1611 (2017).
26. Valentino, R. J. & Van Bockstaele, E. Convergent regulation of locus coeruleus activity as an adaptive response to stress. *Eur. J. Pharmacol.* **583**, 194–203 (2008).
27. Harley, C. W. Norepinephrine and the dentate gyrus. *Prog. Brain Res.* **163**, 299–318 (2007).
28. Loy, R., Koziell, D. A., Lindsey, J. D. & Moore, R. Y. Noradrenergic innervation of the adult rat hippocampal formation. *J. Comp. Neurol.* **189**, 699–710 (1980).
29. Rose, G. M. & Pang, K. C. Differential effect of norepinephrine upon granule cells and interneurons in the dentate gyrus. *Brain Res.* **488**, 353–356 (1989).
30. Seidenbecher, T., Reymann, K. G. & Balschun, D. A post-tetanic time window for the reinforcement of long-term potentiation by appetitive and aversive stimuli. *Proc. Natl. Acad. Sci. USA* **94**, 1494–1499 (1997).
31. Walling, S. G. & Harley, C. W. Locus ceruleus activation initiates delayed synaptic potentiation of perforant path input to the dentate gyrus in awake rats: a novel beta-adrenergic- and protein synthesis-dependent mammalian plasticity mechanism. *J. Neurosci.* **24**, 598–604 (2004).
32. Lovett-Barron, M. et al. Dendritic inhibition in the hippocampus supports fear learning. *Science* **343**, 857–863 (2014).
33. Feng, J. et al. A genetically encoded fluorescent sensor for rapid and specific in vivo detection of norepinephrine. *Neuron* **102**, 745–761 (2019).
34. Takeuchi, T. et al. Locus coeruleus and dopaminergic consolidation of everyday memory. *Nature* **537**, 357–362 (2016).
35. Kempadoo, K. A., Mosharov, E. V., Choi, S. J., Sulzer, D. & Kandel, E. R. Dopamine release from the locus coeruleus to the dorsal hippocampus promotes spatial learning and memory. *Proc. Natl. Acad. Sci. USA* **113**, 14835–14840 (2016).
36. Li, L. et al. Activity-dependent constraints on catecholamine signaling. *Cell Rep.* **42**, 113566 (2023).
37. Howe, M. W., Tierney, P. L., Sandberg, S. G., Phillips, P. E. & Graybiel, A. M. Prolonged dopamine signalling in striatum signals proximity and value of distant rewards. *Nature* **500**, 575–579 (2013).
38. Lohani, S. et al. Burst activation of dopamine neurons produces prolonged post-burst availability of actively released dopamine. *Neuropsychopharmacology* **43**, 2083–2092 (2018).
39. Wagatsuma, A. et al. Locus coeruleus input to hippocampal CA3 drives single-trial learning of a novel context. *Proc. Natl. Acad. Sci. USA* **115**, E310–E316 (2018).
40. Brewin, C. R., Andrews, B. & Valentine, J. D. Meta-analysis of risk factors for posttraumatic stress disorder in trauma-exposed adults. *J. Consult. Clin. Psychol.* **68**, 748–766 (2000).

41. Safari, S. et al. Sex differences in spatial learning and memory and hippocampal long-term potentiation at perforant pathway-dentate gyrus (PP-DG) synapses in Wistar rats. *Behav. Brain Funct.* **17**, 9 (2021).

42. Yagi, S., Lee, A., Truter, N. & Galea, L. A. M. Sex differences in contextual pattern separation, neurogenesis, and functional connectivity within the limbic system. *Biol. Sex. Differ.* **13**, 42 (2022).

43. Bonanno, G. A., Romero, S. A. & Klein, S. I. The temporal elements of psychological resilience: An integrative framework for the study of individuals, families, and communities. *Psychol. Inq.* **26**, 139–169 (2015).

44. Kessler, R. C., Sonnega, A., Bromet, E., Hughes, M. & Nelson, C. B. Posttraumatic stress disorder in the National Comorbidity Survey. *Arch. Gen. Psychiatry* **52**, 1048–1060 (1995).

45. Hunsaker, M. R., Rosenberg, J. S. & Kesner, R. P. The role of the dentate gyrus, CA3a,b, and CA3c for detecting spatial and environmental novelty. *Hippocampus* **18**, 1064–1073 (2008).

46. Prince, L. Y., Bacon, T. J., Tigaret, C. M. & Mellor, J. R. Neuromodulation of the feedforward dentate gyrus-CA3 microcircuit. *Front. Synaptic Neurosci.* **8**, 32 (2016).

Acknowledgements

Author contributions

E.T.Z. performed conceptualization, methodology, investigation, formal analysis, fiber photometry analysis, and writing of the original draft. G.S.S. performed behavioral experiments on immunohistochemistry. J.F. and Y.L. performed conceptualization and experiments relating to the development of the GRAB_NE and GRAB_DA sensors. M.R.B. conceptualized, acquired funding for, and supervised the project, as well as assisted in writing the manuscript.

Competing interests

The authors declare no competing interests.

Additional information

Supplementary information The online version contains supplementary material available at https://doi.org/10.1038/s41467-025-55817-x.

Correspondence and requests for materials should be addressed to Michael R. Bruchas.

Peer review information *Nature Communications* thanks Stephanie Grella, and the other anonymous reviewers for their contribution to the peer review of this work. A peer review file is available.

Reprints and permissions information is available at http://www.nature.com/reprints

Publisher's note Springer Nature remains neutral with regard to jurisdictional claims in published maps and institutional affiliations.